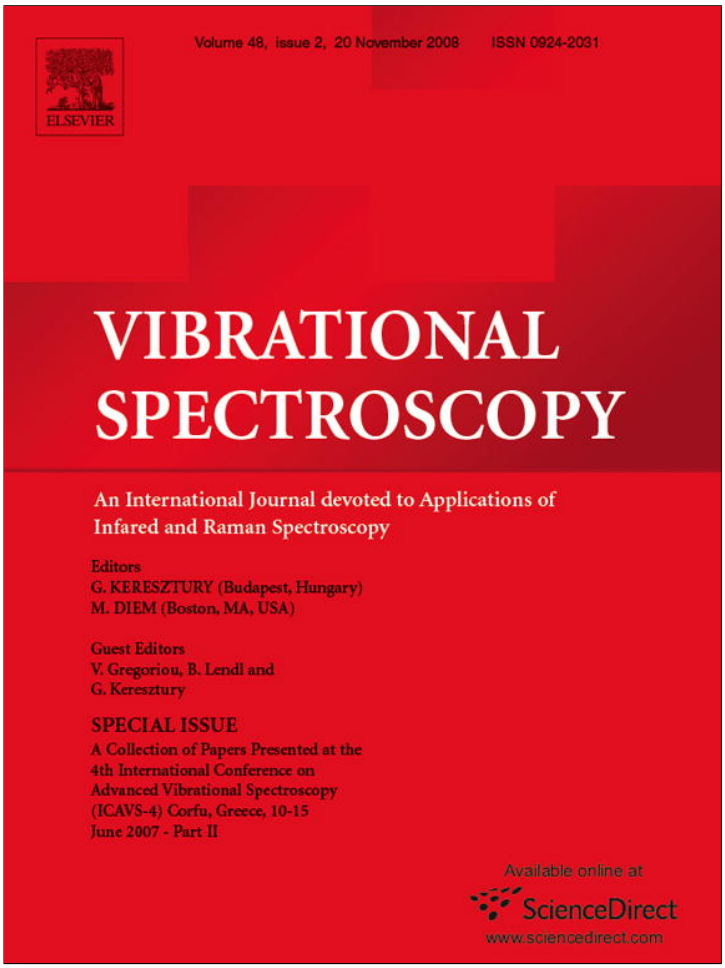

Available online at www.sciencedirect.com
ScienceDirect
Vibrational Spectroscopy 48 (2008) 179–188
VIBRATIONAL SPECTROSCOPY
www.elsevier.com/locate/vibspec

Subcellular localized chemical imaging of benthic algal nutritional content via HgCdTe array FT-IR

Justin N. Murdock [a,b], Walter K. Dodds [b], David L. Wetzel [a,*]

[a] *Microbeam Molecular Spectroscopy Laboratory, Kansas State University, Manhattan, KS 66056, USA*
[b] *Division of Biology, Kansas State University, Manhattan, KS 66056, USA*

Received 11 July 2007; received in revised form 14 November 2007; accepted 17 December 2007
Available online 31 December 2007

Abstract

Algae respond rapidly and uniquely to changes in nutrient availability by adjusting pigment, storage product, and organelle content and quality. Cellular and subcellular variability of the relative abundance of macromolecular pools (e.g. protein, lipid, carbohydrate, and phosphodiesters) within the benthic (bottom dwelling) alga *Cladophora glomerata* (a common nuisance species in fresh and saline waters) was revealed by FT-IR microspectroscopic imaging. Nutrient heterogeneity was compared at the filament, cellular, and subcellular level, and localized nutrient uptake kinetics were studied by detecting the gradual incorporation of isotopically labeled nitrogen (N) (as $K^{15}NO_3$) from surrounding water into cellular proteins. Nutritional content differed substantially among filament cells, with differences driven by protein and lipid abundance. Whole cell imaging showed high subcellular macromolecular variability in all cells, including adjacent cells on a filament that developed clonally. N uptake was also very heterogeneous, both within and among cells, and did not appear to coincide with subcellular protein distribution. Despite high intercellular variability, some patterns emerged. Cells acquired more ^{15}N the further they were away from the filament attachment point, and ^{15}N incorporation was more closely correlated with phosphodiester content than protein, lipid, or carbohydrate content. Benthic algae are subject to substantial environmental heterogeneity induced by microscale hydrodynamic factors and spatial variability in nutrient availability. Species specific responses to nutrient heterogeneity are central to understanding this key component of aquatic ecosystems. FT-IR microspectroscopy, modified for benthic algae, allows determination of algal physiological responses at scales not available using current techniques.

Keywords: Algae; Fourier transform infrared; Mapping; Macromolecular pools; Nitrogen; Periphyton; Algal stoichiometry

1. Introduction

Algae growing on the bottom of aquatic habitats (i.e. benthic algae) play a major role in ecosystem energy flow in all shallow lighted habitats such as streams, shallow lake bottoms, estuaries, wetlands, and coastal marine habitats. These algae take up inorganic nutrients from the water, metabolize them into organic form, and transfer the nutrients to the organisms that eat them. Benthic algae often responsed to excessive nutrient input with extreme growth that may harm water quality and other aquatic organisms [1,2]. Current methods limit the distinctions of *in situ* algal stoichiometric responses to nutrient availability to a whole community scale because they depend upon quantitative analysis of macro-scale quantities (e.g. deciliters of water or milligram of tissue). Species have evolved unique growth responses to changing environmental nutrient availability by adjusting cellular content and quality of macromolecular pools devoted to pigments, storage products, and organelles. Understanding species-specific growth responses to changes in stream nutrient concentrations will assist in predicting how algal assemblages will change with increased human-induced nutrient loadings, as well as describing the basic ecological interactions among these organisms.

Algal nutritional analysis with Fourier transform infrared (FT-IR) microspectroscopy is a quickly expanding area and has been applied to the analysis of cultured single cell and colonial algae [3–6], and natural phytoplankton (algae suspended in the water column) communities in lake [7–9] and marine [10] environments. FT-IR algal investigations have focused on the cellular response of major organic functional groups, or macromolecular pools (e.g. proteins, lipids, carbohydrates, and

* Corresponding author.
E-mail address: dwetzel@ksu.edu (D.L. Wetzel).

0924-2031/$ – see front matter © 2008 Published by Elsevier B.V.
doi:10.1016/j.vibspec.2007.12.011

phosphodiesters), to changing environmental nutrient concentrations. Measurable responses have been observed in diatoms [4,10], green algae [5,7], and cyanobacteria [8,11]. For example, nitrogen limitation in algae often causes decreases in protein, and increases in lipid and carbohydrate content [10]. Currently, most analyses have been done with individual spectra within spatial areas from approximately 10 to 30 μm^2, or line mapping. Since algal cell sizes can differ by an order of magnitude among species and cellular content is often distributed across a heterogeneous matrix throughout the cell, whole cell/colony imaging may provide a more accurate determination of whole cell/colony responses to micro- and macro-habitat environmental change.

Benthic algae and phytoplankton develop in different nutritional environments. Benthic algae grow in a three-dimensional matrix attached to a surface (e.g. rocks, sediment, aquatic plants, or other benthic algae) (Fig. 1), and obtain nutrients from water passing over or through the mat, or mineralized from nearby algae. As algal mats develop, space separating individual algae decreases and inter- and intraspecific competition for nutrients increases. Enhanced competition and variable nutrient diffusion rates into mats create patchy microenvironments unique to benthic algal communities. This environmental variability can translate into nutritional variability within the community [12] and may extend to nutritional heterogeneity in individual algal filaments, colonies, or cells.

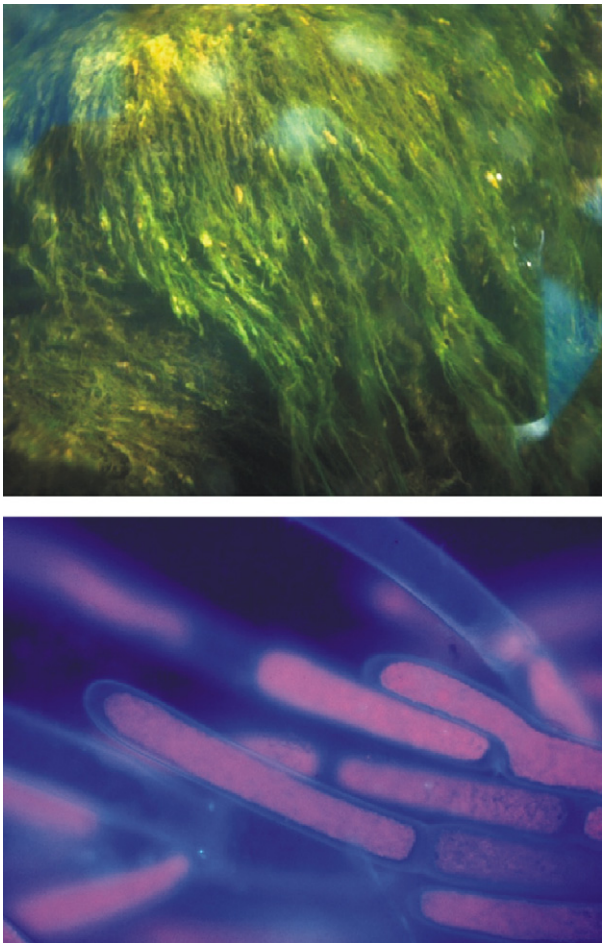

Fig. 1. (Top) The benthic alga *Cladophora glomerata* growing in a stream (the small specks in the filaments are snails that are approximately 5 mm long); (bottom) photomicrograph of filaments (cells are approximately 200 μm long). In the electronic version, cell walls are stained blue with the fluorochrome Calcofluor, and the red within the cell is chlorophyll autoflourescence. Note the branching pattern of filaments.

The goal of this study was to assess the applicability of FT-IR microspectroscopic imaging to detect nutritional heterogeneity and nutrient uptake in benthic algae at the filament, cellular, and subcellular level. Adjustments to current phytoplankton sample preparation techniques were implemented to study the macromolecular pool distribution in the filamentous alga *Cladophora glomerata*. Nutrient uptake kinetics was studied by localizing the incorporation of ^{15}Nitrogen (as $K^{15}NO_3$) into cellular proteins [11,13]. *Cladophora* has proliferated in streams globally due to increased nutrient loading, and can often reach nuisance levels [14]. Excessive growth decreases streambed habitat, food resources, and water quality for other aquatic organisms, clogs municipal water intake pipes, and decreases stream recreational value [1]. More information is needed on the physiological response of *Cladophora* to nutrient pollution to help mitigate excessive growth.

2. Experimental

2.1. Sample collection and processing

Rocks dominated by natural assemblages of the green filamentous alga *C. glomerata* were collected from a shallow prairie stream on the Konza Prairie Biological Station (KPBS) near Manhattan, KS, USA. KPBS is a 1637 ha pristine tallgrass prairie ecosystem containing low nutrient headwater streams that are minimally disturbed by human influences. In the laboratory, five rocks were placed into each of two 22 L recirculating chambers filled with low nitrogen stream water (~7.2 μmol total N, ~0.65 μmol nitrate, <0.28 μmol ammonium), and incubated for 4 days under constant light (~300 μmol quanta m^{-2} s^{-1} photosynthetically available radiation supplied by fluorescent lights). Chambers were spiked daily with either 0.32 mmol of $K^{14}NO_3$ or $K^{15}NO_3$, the amount of nitrogen taken up by a similar amount of benthic algae in a 24 h period (Murdock, unpublished data). Additionally, 0.012 mmol of KH_2PO_4 was added daily to prevent phosphorus limitation of algal growth.

Filaments were gently removed with forceps at the point of attachment from rocks and rinsed three times with deionized water [7]. Cells were examined under light microscopy to determine if cell walls or cellular contents were physically changed due to possible ionic imbalance from rinsing [8]. No visible changes were observed. To create areas of single cell layers required for analysis, filaments were placed on an IR reflective (Low-e) slide (Kevley Technology, Chesterfield, OH, USA) with a few drops of deionized water to float the filaments and allow even spreading of the filament branches. Excess water was slowly removed with a pipette and slides were dried in a desiccator for approximately 12 h. Slides were reexamined to check for physical changes in cellular content distribution due to drying. Some cells had expelled portions of their cellular

content, but most appeared intact and minimally altered. Spectra were recorded from only unchanged cells.

2.2. Spectra and map acquisition

Samples were analyzed with a PerkinElmer Spotlight 300 FT-IR microspectrometer with a 16 element mercury–cadmium–telluride (MCT) pushbroom focal plane array producing a rectangular (x, y) image. The optical arrangement results in a projection of the detector elements that provide a minimum nominal pixel size of 6.2 μm × 6.2 μm. This optical arrangement was used to obtain reflection absorption spectra of whole algal cells. Additionally, individual spectra were obtained in single detector mode from the center of randomly selected cells along a filament using a nominal pixel size of 25 μm × 25 μm.

Spectra were colleted from 4000 to 700 cm^{-1} with a spectral resolution of 4 cm^{-1}, and 64 scans co-added. Background spectra were obtained from a clean section of the IR reflective slide. A constant sample temperature of 21 °C was maintained during spectra collection. Image absorption spectra were baseline corrected using Spectrum V. 5.3.1 (PerkinElmer).

Macromolecular bands of interest were amides I and II (1655 cm^{-1} and 1545 cm^{-1}, respectively), lipid carbonyl (2927 cm^{-1}) and CH_2 (1729 cm^{-1}), carbohydrate (1025 cm^{-1}), and phosphodiester P═O (1240 cm^{-1}) as stated in Table 1. The enhanced CH_2 stretch vibrational band at 2927 cm^{-1} that accompanies the 1729 cm^{-1} carbonyl band was used to image lipid content because the larger peaks allowed for better area differentiation among spectra [15]. Peak areas of the 1729 cm^{-1} band in close proximity of the amide I band were less reliably determined in this application. Bands monitored in this study were identified in the previous algal and bacterial FT-IR studies of Naumann [16], Giordano et al. [10], Sigee et al. [7], and Heraud et al. [17].

Spectra from the center of 15 individual cells were randomly collected along the length of each filament, and images of six complete *Cladophora* cells (~75 μm × 200 μm per cell, containing approximately 300 individual spectra per cell) were produced. Cell to cell distances along a filament were measured from brightfield photomicrographs of whole filaments using Image J digital image analysis software [18]. Cell distance was measured as the linear distance from the point of spectral collection along the filament and branches to the point the filament attached on the rock.

2.3. Data analysis

The absorption bands of protein, carbohydrate, lipid, and phosphodiester from individual spectra of cells along a filament were compared with (1) hierarchical cluster analysis using Ward's method and Pearson's correlation coefficient distances, and (2) principal component analysis (PCA) to explore intracellular nutritional variability [16,19]. Baseline corrected peak areas were calculated from the band area at the wavenumber ranges stated previously for each macromolecular pool.

Rectangular (x, y) images of whole cells were used to explore subcellular nutritional variability. Principal component analyses were used to delineate areas of contrasting macromolecular composition within whole cell images. PCA factor images were produced using data from the fingerprint region and CH_2 stretching vibrational region of each spectra within a cell at a pixel size of 6.2 μm × 6.2 μm. Factor scores were plotted to show spatial heterogeneity of nutritional content, and loading plots indicated which absorption bands were driving subcellular differences [8].

^{15}N uptake by cells was measured through a shift in the amide II peak. A change in the peak frequency provided rudimentary evidence of ^{15}N incorporation into cellular proteins. An initial estimate of ^{15}N incorporation was made by calculating the ratio of the resultant amide II peak height at 1535 cm^{-1} to the original ^{14}N amide II peak height at 1545 cm^{-1}. The wavenumber of the ^{14}N amide II peak (1545 cm^{-1}) was determined as the average amide II peak location from 20 *Cladophora* cells from the $K^{14}NO_3$ treatment. This method was used to create whole cell images of ^{15}N incorporation.

Table 1
Point spectra (intercellular) summary statistics for macromolecular peak areas and peak ratios (n = 50 cells)

	Wavenumber (cm^{-1})	Assignment	Minimum	Maximum	Mean	CV
Peak areas						
Lipid (as straight chain CH_2)	2927	C–H stretch of CH_2 (asymetric)	8.33	38.4	22.0	0.37
Protein (amide I)	1655	C═O stretch of amide I	5.72	33.0	18.5	0.36
Protein (amide II)	1545	N–H bend and C–N stretch of amide II	0.24	13.1	6.12	0.53
Carbohydrate	1025	C–O–C stretch of pollysaccharides	7.85	93.8	55.3	0.39
Phosphodiester	1240	P═O stretch (symmetric) of polyphosphate storage products, phosphoralated proteins, DNA, RNA	3.06	15.7	8.15	0.32
Peak ratios						
Amide I/lipid			0.51	1.16	0.85	0.16
Amide I/carbohydrate			0.12	1.32	0.41	0.65
Amide I/phosphodiester			0.95	7.03	2.47	0.50
Lipid/carbohydrate			0.15	2.10	0.49	0.70
Lipid/phosphodiester			1.07	9.21	2.97	0.52
Carbohydrate/phosphodiester			1.92	19.6	7.18	0.49

Peak modeling was used as an alternative quantitative approach to measure ^{15}N uptake. Fourier self-deconvolution was applied to individual spectra from the ^{15}N treatment to enhance the resolution of the separate ^{14}N and ^{15}N peaks in the amide II band. The ^{14}N and ^{15}N peaks were modeled using Gaussian and Lorentzian curve fitting with an iterative curve fitting process (Grams/AI Version 7.02, Thermo Scientific, Waltham, MA, USA) using a full width at half height (FWHH) of 10, and the area under each peak was determined. The ratio of the shifted peak area to the original peak area was used as the measure of ^{15}N incorporation. Linear regression analysis was used to compare nutrient content and cell location along the filament to the magnitude of ^{15}N uptake.

3. Results

3.1. Nutrient variability

3.1.1. Differences among cells

Macromolecular pools were highly variable among spatially disparate *Cladophora* filaments (cm apart), as well as among cells within a single filament (mm apart) (Table 1). However, the variability of each nutrient pool was similar (CV ranged from 32 to 53%, Table 1). Cluster analyses based on macromolecule peak areas separated cells into three distinct groups, and into four groups based on peak area ratios. However, there was no apparent meaningful grouping variable such as distance apart on a filament or day filament was sampled. Principal component analysis also did not differentiate cells by nutritional content based on peak area or peak ratio. Despite a lack of spatial differentiation, some trends in *Cladophora* cellular content were evident.

There was a considerable difference in the co-occurrence of macromolecular pools among all *Cladophora* cells. The amide I (protein) and lipid bands had a strong positive correlation ($r = 0.91$, $n = 50$), while carbohydrate correlations with proteins and lipids were weaker, but still significant. Phosphodiester content had only a weak correlation with carbohydrates ($r = 0.34$, $n = 50$) (Table 2). A multivariate comparison of macromolecular pool composition among cells with PCA further supported the importance of protein and lipid

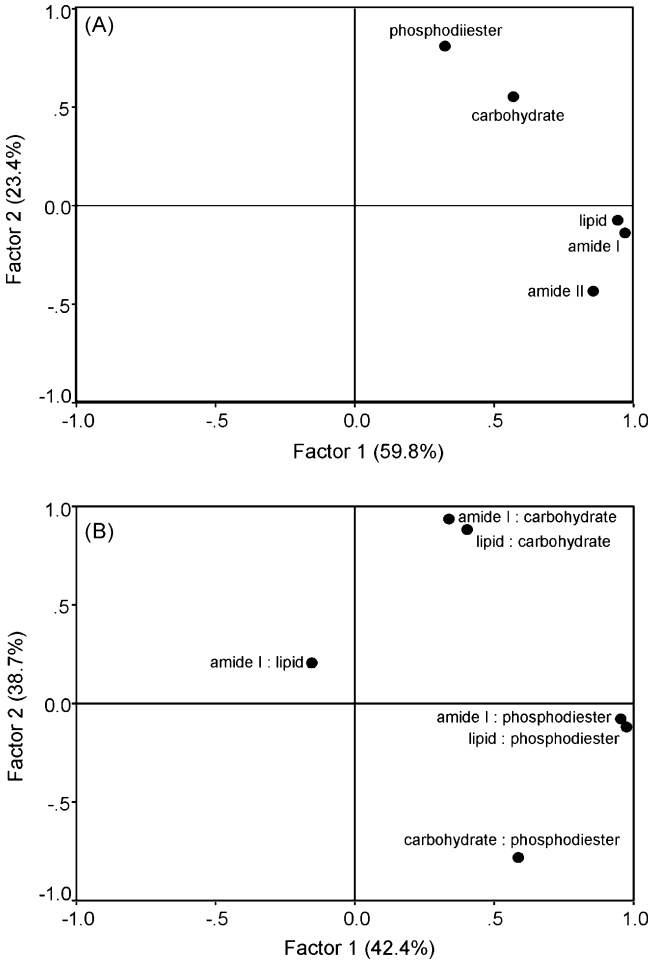

Fig. 2. PCA biplots of the factors 1 and 2 of (A) macromolecular pool peak areas, and (B) peak area ratios in individual *Cladophora* cells (point measurements, $n = 50$). The first two factors were driven by lipid and protein content and explain 83% of the macromolecular pool variability and 81% of the pool ratios among cells.

in differentiating *Cladophora* cells. The first two factors accounted for 83.2% of the nutrient variation (factor 1, 59.8%). Factor 1 was characterized by the dominance of proteins and lipids, with factor 2 dominated by high carbohydrates and phosphodiesters (Fig. 2A). A PCA of nutrient ratios among

Table 2
Point spectra (intercellular) macromolecular peak area correlation coefficients

	Lipid	Protein (amide I)	Protein (amide II)	Carbohydrate	Phosphodiester
Lipid	–	**0.906** ***0.0000***	**0.767** ***0.0000***	**0.475** ***0.0004***	0.232 *0.1020*
Protein (amide I)		–	**0.887** ***0.0000***	**0.419** ***0.0022***	0.241 *0.0889*
Protein (amide II)			–	0.198 *0.1627*	−0.003 *0.9837*
Carbohydrate				–	**0.340** ***0.0147***
Phosphodiester					–

Pearson correlation coefficients ($n = 50$) (two-tailed significance). p-Values are in italics below the correlation coefficient. Bold values are significant at $p = 0.05$.

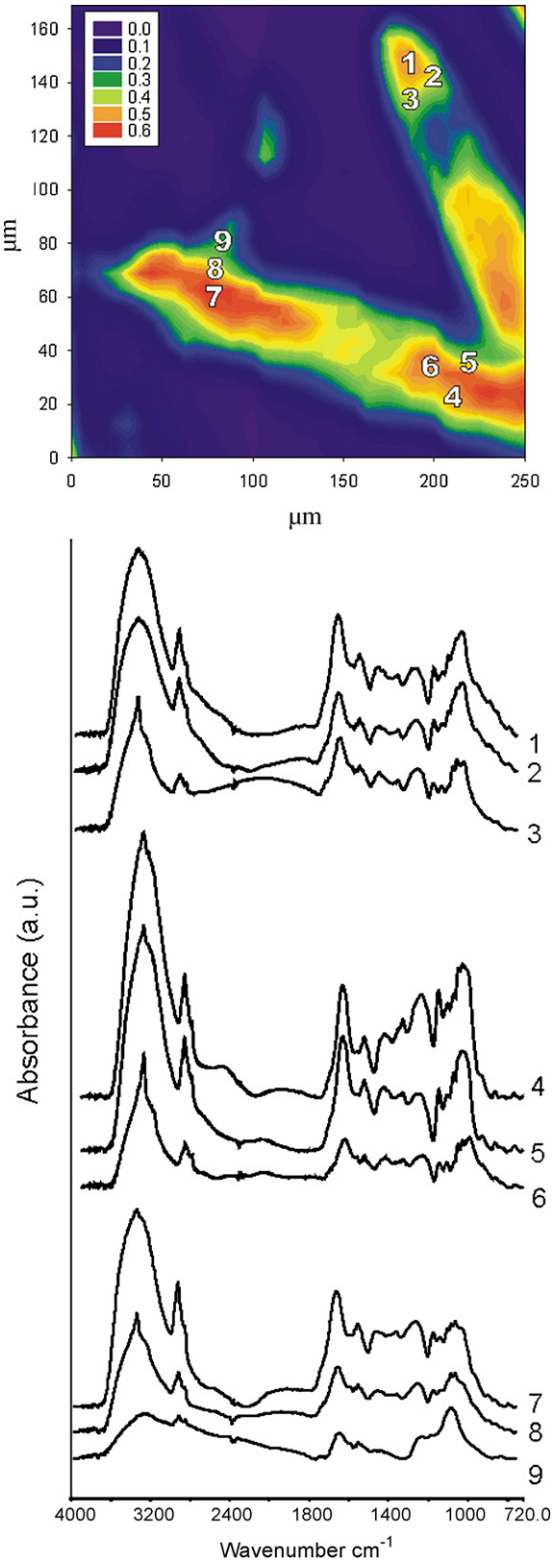

Fig. 3. Rectangular *x*, *y* Grahm–Schmidt function (total absorbance intensity) image of two *Cladophora* cells. Three individual spectra from three areas (9 total) show the high variability in macromolecular pools that occur within and between two adjacent cells. Spectra 9 is of a diatom growing attached to the side of the *Cladophora* cell and is visibly distinct, containing a much higher lipid:protein ratio than the larger green alga and a distinct silica band at 1080 cm^{-1}. In the web version, red areas in all spectral images denote areas of higher absorbance, and purple areas indicate low absorbance.

cells showed a close relationship of protein and lipid content remained relatively constant, and intracellular variation appeared to be driven by changes in the proportions of carbohydrate and phosphodiester concentrations relative to lipid and protein (Fig. 2B).

3.1.2. Subcellular differences

Subcellular imaging of entire *Cladophora* cells showed evidence of high nutritional variability within a cell. For example, Fig. 3 illustrates that discrete measurements in a single cell can produce different spectra at the base, middle, and tip. When adjacent cells were imaged, distinct differences in individual macromolecular pool distribution were evident. Notice in Fig. 4 that high phosphodiester content that occurred in one cell was absent in the other. Carbohydrate concentrations were high in the base and tip of the cells, but were more evenly distributed throughout the cell than the other components. Despite these differences some subcellular patterns were evident. Similar to intracellular patterns, the location of protein and lipid concentrations were coincident in both cells. Also, subcellular images showed that the overall concentration of nutritional pools was consistently greater at terminal ends of cells and at the nodes of adjoining cells.

Subcellular imaging of nutritional ratios revealed nutrient co-occurrence in *Cladophora* cells. In Fig. 5, macromolecular peak ratio images show the cell perimeter is dominated by lipids, evidenced by the high lipid:carbohydrate and lipid:protein content. In contrast, the interior contains areas of high protein and phosphodiester concentration. These images confirm that nutrient ratios within single cells can be at least as spatially variable as individual macromolecular pools.

Principal component analysis further delineated the spatial distribution of the complex combinations of all macromolecular pools within a cell. Fig. 6 shows PCA factor images and spectra loadings of three separate cells (A, B, and C) for factors 2 (top image in each pair of images) and 3. Factor 1 was driven by physical differences within the cell and was not considered. All cells showed a defined perimeter that had a very different chemical makeup than the center. In cells (A) and (B) this perimeter was dominated by lipids and carbohydrates, while C's perimeter contained high carbohydrate but low lipid content. Distinct areas dominated by proteins are evident in all cells in factor 3 images.

Imaging adjacent cells (as done in Figs. 4–6) shows that in natural benthic algal communities, cells of the same species that are only mm apart can vary substantially in their nutritional heterogeneity. The spatial resolution of this technique also allowed the distinction of different algal species physically touching one another, e.g. the discrete spectra of a diatom attached to a *Cladophora* cell was resolved in spectrum 9 of Fig. 3.

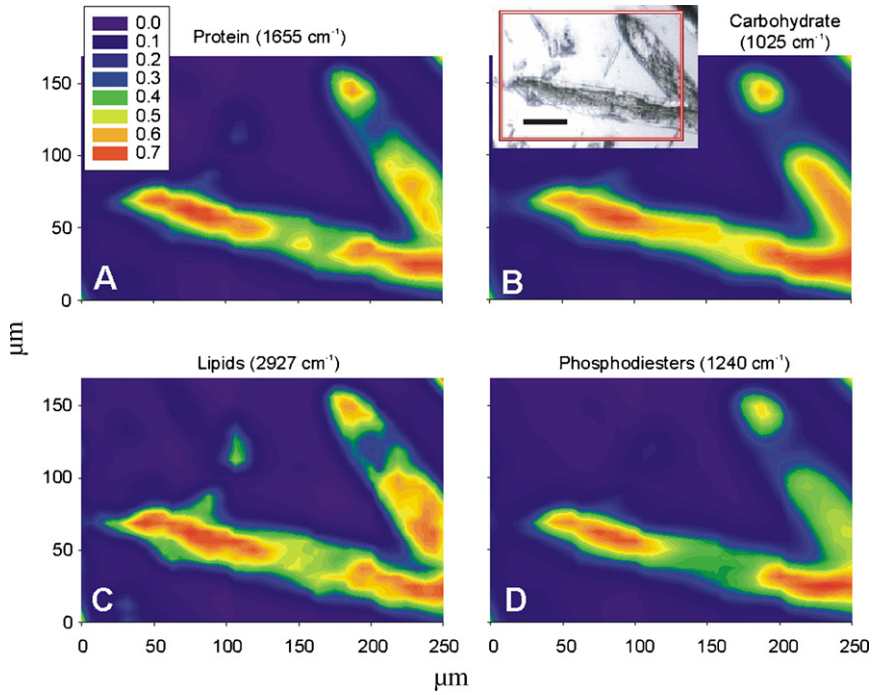

Fig. 4. *x*, *y* images of the subcellular distribution of individual macromolecular pools of (A) protein ~1645 cm^{-1}, (B) carbohydrate ~1025 cm^{-1}, (C) lipid ~2927 cm^{-1}, and (D) phosphodiesters ~1240 cm^{-1} within the two *Cladophora* cells from Fig. 3 at 6.2 µm × 6.2 µm nominal pixel size. The scale box in panel (A) is absorbance intensity and frame in the photomicrograph indicates the area imaged. Note the locus at protein concentration is coincident with that of the lipid, but that the carbohydrates are more widely distributed throughout the cells.

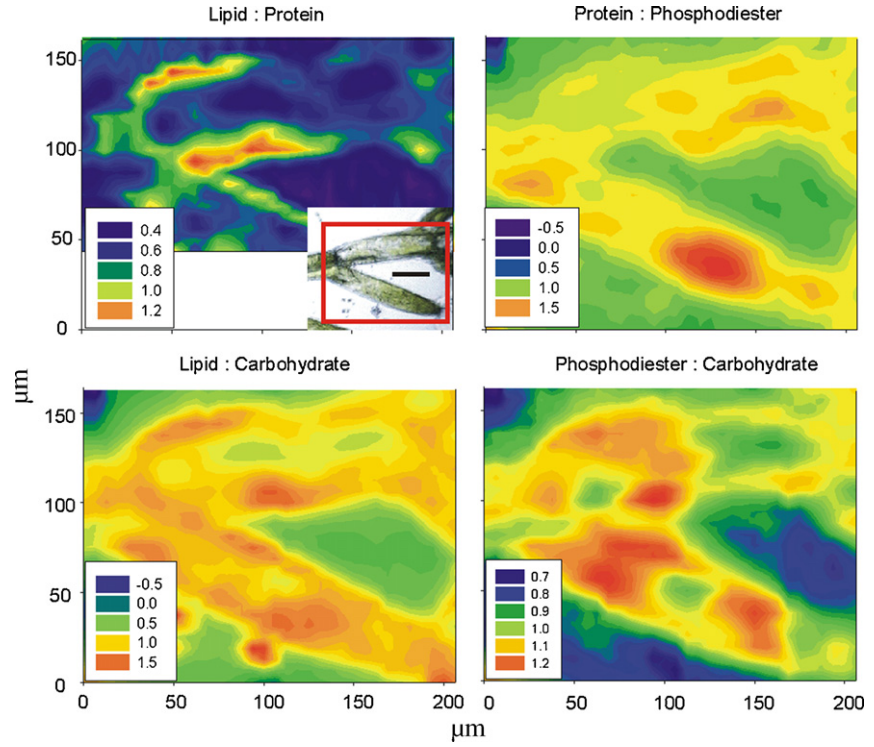

Fig. 5. Example of macromolecular ratio images of two adjacent *Cladophora* cells. The upper cell in each image is a thallus cell and the lower cell a branch tip. Scale boxes are absorbance intensity and the box in the photomicrograph indicates the area imaged. Note the high lipid content near the cell walls, and the protein hotspot in the tip cell. Carbohydrates appear slightly higher in the thallus cell.

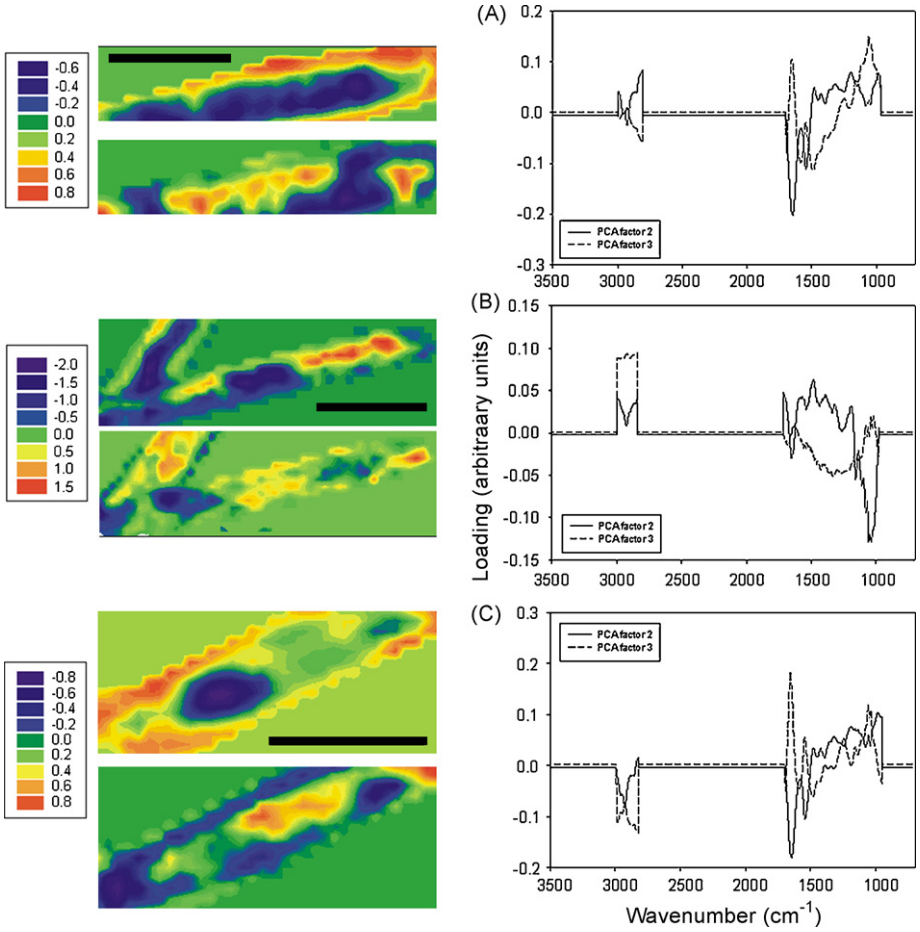

Fig. 6. PCA factor images of three *Cladophora* cells using the spectrum range of 3000–2900 cm^{-1} and 1750–900 cm^{-1} and corresponding loading plots for factors 2 and 3. In each pair of images, factor 2 is on top. Scale bars are 100 μm.

3.2. Nitrogen uptake

3.2.1. Differences among cells

^{15}N incorporation in *Cladophora* cells was observed as a shift in the amide II peak from 1545 to 1535 cm^{-1}. There was an average peak shift of 7 cm^{-1} (to 1538 cm^{-1}) after 3 days, and 10 cm^{-1} (to 1535 cm^{-1}) after 4 days (Fig. 7A). As the heavier ^{15}N isotope was incorporated into amine group proteins there was a reduction in the 1545 cm^{-1} peak and increase in the 1535 cm^{-1} peak. An intermediate peak appeared at 1541 cm^{-1} at the position of an original amide II shoulder; however it vanished upon spectral subtraction of the original ^{14}N spectra. Thus, this artifact was disregarded. A gradual progression of the amide II peak towards 1535 cm^{-1} was evidenced by a frequent peak doublet appearing in spectra from days 3 and 4 during the incorporation of the ^{15}N isotope. Fourier self-deconvolution sharpened the ^{14}N and ^{15}N peaks in the amide II band (Fig. 7B) and second derivative spectra clarified the existence of separate peaks (Fig. 7C). Several spectra with single amide II peaks at 1535 cm^{-1} were observed after 4 days indicating that some proteins had become completely labeled with ^{15}N by this time. No change in the peak position was detectable in day 1 or 2 spectra.

Amide II ^{15}N:^{14}N peak height ratios provided a cursory indicator of the extent of ^{15}N uptake. However, curve modeling was chosen for quantification and resulted in mean ratios of 0.93 (S.D. 0.5) and 1.75 (S.D. 1.2) for days 3 and 4 individual spectra, respectively. Amide II ^{15}N:^{14}N peak height ratios were less subjective and less variable between cells, but showed weaker relationships with cell macromolecular pools.

On day 4, ^{15}N uptake by a *Cladophora* filament exhibited an exponential relationship with distance from the point of attachment (Fig. 8). Less than 3 mm from the rock, cells had a consistent 1:1 peak area ratio of ^{15}N to ^{14}N, but exhibited a 5-fold increase from 3 to 4 mm. Nutritional relationships with the modeled ^{15}N ratios were weak, with the strongest being a positive linear relationship with phosphodiester content ($r^2 = 0.34$, $n = 29$). The other constituents only showed a weak positive relationship with ^{15}N after day 4, e.g. lipid ($r^2 = 0.21$), and protein (amide I, $r^2 = 0.26$).

3.2.2. Subcellular differences

Whole cell images of ^{15}N content were produced to show where N was most readily incorporated within the cells, and representative images are displayed in Fig. 9. Intensity values corresponds to the ratio of the ^{15}N (1535 cm^{-1}) to ^{14}N

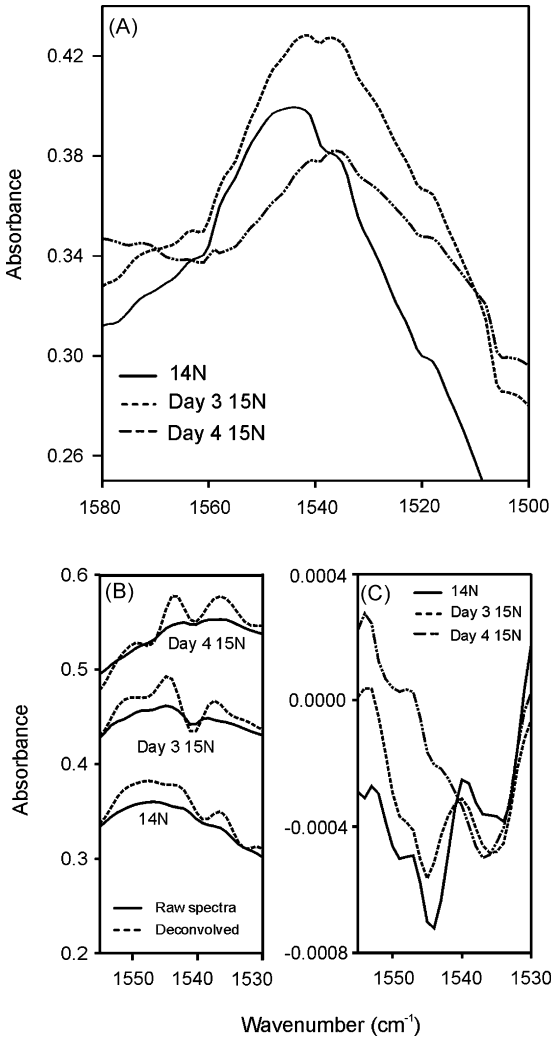

Fig. 7. (A) Average of the amide II peak absorbance from cells incubated in ^{14}N and after 3 and 4 days in ^{15}N. The peak shifted shows a progression of protein labeling over time. (B) Raw and Fourier self-deconvolved spectra typical of ^{14}N, day 3 ^{15}N, and day 4 ^{15}N enhancing the change in height of the 1545 and 1535 cm^{-1} peaks with increased ^{15}N incorporation. (C) The second derivatives of spectra in panel (A). Note the change in the 1545 cm^{-1}:1535 cm^{-1} peak heights between the ^{14}N and day 4 ^{15}N spectra.

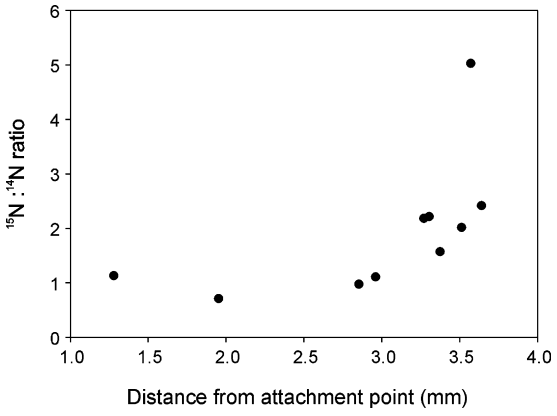

Fig. 8. Relationship between the location of a cell on a filament (in relation to the filament attachment point) and the amount of ^{15}N incorporated into the cell after 4 days of incubation in $K^{15}NO_3$. ^{15}N uptake was substantially higher >3 mm from the filament attachment point.

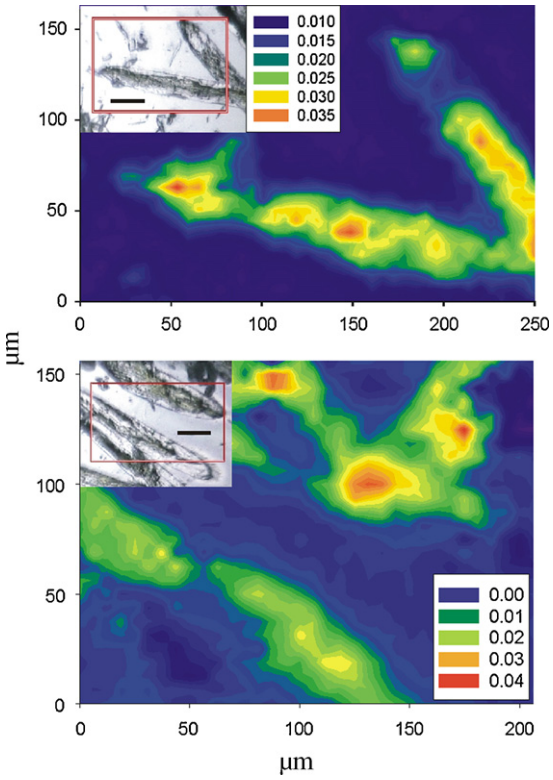

Fig. 9. Two subcellular *x*, *y* images of localized ^{15}N incorporation. Red squares in each photomicrograph denote the area imaged. Scale boxes indicate the $^{15}N/^{14}N$ peak height ratio in cellular proteins and indicates areas of higher ^{15}N incorporation.

(1545 cm^{-1}) peak heights. Peak height ratios were used because modeling of the hundreds of individual spectra that make up each image was not feasible in this study. Although the cells in each image developed very close together, they have taken up different amounts of ^{15}N, and incorporated it into different locations. When compared to the protein distribution of these cells (Fig. 4), it is apparent that ^{15}N uptake did not necessarily coincide with areas of elevated protein concentration. Additionally, there was no coincidence of ^{15}N uptake with areas of high protein:lipid content at a subcellular level. Because whole cell images were taken from different filaments it was not possible to compare ^{15}N uptake and distance relationship at the subcellular level beyond two adjacent cells.

4. Discussion

Cladophora filaments that developed in a natural stream had an extremely patchy nutrient distribution. Cells could not be differentiated by spatial distance or cell type based on nutritional content using a nominal pixel size of 25 µm × 25 µm (approximately one fourth to one third the area of the cell). Thus we were unable to determine if some filaments, or cells along a filament, were nutritionally 'healthier' than others. However, we were able to define which macromolecular pools (i.e. lipids and proteins) were highly correlated among *Cladophora* cells, and that lipid and protein

content were also driving subcellular variability within this species.

Subcellular imaging of the macromolecular pool distribution provided insight into the lack of intracellular patterns seen from discrete spectra. The finding that genetically identical, adjacent cells had very different subcellular nutrient content and distribution suggests that consistent nutritional spatial patterns may not exist. It also emphasizes the highly plastic stoichiometric nature of this species. We found that spectra from single points in *Cladophora* cells can be very different at high spatial resolution (e.g. Figs. 3 and 4). Thus taking spectra in the middle of the cell without considering cell wall content or areas of rapid growth can potentially give results that do not accurately reflect the nutritional content of the entire cell. The appropriate nominal pixel size and spectral collection location will likely vary between inter- and intracellular investigations of different algal species.

One distinct pattern often seen in whole cell images was a higher concentration of total nutritional content at the ends of the cells. *Cladophora* filaments grow through apical (branching) and intercalary (cell lengthening) growth, and the dominant growth pathway is greatly dependent on environmental conditions [20]. Thus, accumulation of macromolecular pools at the branch apical tips, and cellular nodes would correspond to keeping nutrients in portions of the cell with high-energy demand.

In *Cladophora*, proteins are mainly associated with chloroplasts and nuclei, lipids with cell and thykaloid membranes, carbohydrates with starch storage products and cellulose cell walls, and phosphorus with nuclei and polyphosphate storage products [17]. Cells are multi-nucleated with chloroplasts evenly distributed throughout the intercellular space. Contents can also shift depending on cell state and light availability [20]. PCA factor images and nutrient ratio images of whole cell lipid, protein, and carbohydrate locations were consistent with these known nutrient distributions. Due to the relatively complex composition of algal cellular components, a somewhat heterogeneous distribution of macromolecular pools within *Cladophora* cells was expected. However, the high nutritional variability between adjacent cells, i.e. cells that were created by cloning, was not anticipated a priori.

A temporal progression of ^{15}N incorporation into cellular proteins was evidenced by a doublet in the amide II peak region. This suggests that some proteins had incorporated ^{15}N and some had not. As a greater proportion of the proteins became labeled, the lower frequency peak got taller while the higher frequency peak decreased, causing an overall shift in the amide II peak as more ^{15}N was incorporated into cellular proteins [21]. The amide II shift was similar to that observed by Kimura et al. [21] in cyanobacterial cells fully labeled with ^{15}N. This trend was more pronounced from the deconvolved spectra where a progression through three frequencies became evident.

Calculations of peak areas through modeling provided ^{15}N ratios that better coincided with cellular nutrient content and N uptake than the preliminary direct measurements of peak heights of the raw spectra. The use of this method to obtain ^{15}N to ^{14}N ratios shows promise. Since execution of this method relies on the subjective selection of curve fitting parameters, and the vibrational contributions to the amide II band have not been as well studied as the amide I band, more data sets are needed to refine selection of parameter values for modeling the amide II band. Further investigation of N uptake from different sources (i.e. ammonium and dissolved organic N) is also warranted.

Whole cell imaging provided individual cell physiological responses by localizing subcellular N incorporation. Our observation that N uptake did not correlate with regions where proteins were most concentrated suggests that other cell constituents, such as amino acids [22], are initially taking up N throughout the cell. Localizing N uptake can provide insight into where nutrient microenvironmental hotspots are occurring and how cells close to this region respond compared to cells in less nutrient replete areas of the mat.

External nutrient availability regulates internal algal nutrient content [23], yet it is difficult to analytically detect differences in dissolved nutrient concentration in the water at scales relevant to individual cells. The high nutrient variability within adjacent cells suggests the existence of sub-millimeter and possibly sub-micrometer nutrient microenvironments within benthic algal mats. This finding supports previous studies that proposed the existence of microscale nutrient gradients due to microscale differences in water velocity [24], substratum topography [25], and light availability [26] within benthic algal mats. Whole cell, spatially resolved imaging of nutritional content has potential to help predict nutrient availability within different portions of a benthic algal mats given different environmental conditions.

Previous work on phytoplankton using individual point spectra has illustrated very good differentiation among different species and among single species exposed to nutrient replete or depleted environments [8–10]. However, since phytoplankton are suspended in the water column, regardless of if they are cultured or taken from natural communities, they are exposed to more homogeneous ambient nutritional conditions than are algae in benthic mats. Thus studying benthic algal communities requires a modified approach in both sample preparation and cellular spectral measurement to best reveal response patterns. Imaging the subcellular distribution of single cell and filamentous phytoplankton will shed light on the influence of nutrient availability in benthic mats on intracellular nutrient heterogeneity.

Current FT-IR microspectroscopy allows a relatively fast image acquisition time for entire cells (less than 1 h per 75 μm × 200 μm cell at relatively high spatial and spectral resolution), which is needed to accurately characterize larger algal cells grown in heterogeneous environments. This method is still limited to algal species that do not change physical cell shape when dehydrated. For example, whereas *Cladophora* appeared to maintain even distribution of cell contents upon drying, we observed two other species of green filamentous algae, *Ulothrix* spp. and *Spirogyra* spp. that did not. Methods have been developed to analyze live, hydrated phytoplankton cells [17]. Development of similar methodology for benthic algae will enable more accurate subcellular measurements and whole community analysis.

FT-IR microspectroscopy has great potential in helping to understand benthic microbial ecology. Determination of individual cell and subcellular stoichiometric ratios can partition the contribution of certain species/cells, to the removal of nutrients from the surrounding water, and determine if all cells in a filament or colony have a similar response. Most lakes, streams, and wetlands have a substantial benthic algal component, and attached algae are also important in biofouling in lighted aquatic environments. A stronger understanding of environmental conditions experienced by individual cells of attached algae may ultimately offer insights into the ecology and management of these organisms.

Acknowledgements

We thank Hicran Koc and Hayes Charles for FT-IR microspectroscopy technical assistance in the early stages of this experiment, and Dolly Gudder and two anonymous reviewers for comments on the manuscript. Funding for this research was provided by the Kansas State University Microbeam Molecular Spectroscopy Laboratory and the National Science Foundation (DEB-0416126). Contribution no. 08-1-J Kansas Agricultural Experiment Station, Manhattan.

References

[1] W.K. Dodds, E.B. Welch, J.N. Amer, Benthol. Soc. 19 (2000) 186.
[2] V.H. Smith, Environ. Sci. Pollut. Res. Int. 10 (2003) 126.
[3] J. Beardall, T. Berman, P. Heraud, M.O. Kadiri, B.R. Light, G. Patterson, S. Roberts, B. Sulzberger, E. Sahan, U. Uehlinger, B. Wood, Aquat. Sci. 63 (2001) 107.
[4] K. Stehfest, J. Toepel, C. Wilhelm, Plant Physiol. Biochem. 43 (2005) 717.
[5] C.J. Hirschmugl, Z.E. Bayarri, M. Bunta, J.B. Holt, M. Giordano, Infrared Phys. Technol. 49 (2006) 57.
[6] Y. Liang, J. Beardall, P. Heraud, Bot. Mar. 49 (2006) 165.
[7] D.C. Sigee, A. Dean, E. Levado, M.J. Tobin, Eur. J. Phycol. 37 (2002) 19.
[8] A.P. Dean, D.C. Sigee, Eur. J. Phycol. 41 (2006) 201.
[9] A.P. Dean, M.C. Martin, D.C. Sigee, Phycologia 46 (2007) 151.
[10] M. Giordano, M. Kansiz, P. Heraud, J. Beardall, B. Wood, D. McNaughton, J. Phycol. 37 (2001) 271.
[11] T. Noguchi, M. Sugiura, Biochemistry 42 (2003) 6035.
[12] W.K. Dodds, J. Phycol. 39 (2003) 840.
[13] P.I. Haris, G.T. Robillard, A.A. Vandijk, D. Chapman, Biochemistry 31 (1992) 6279.
[14] W.K. Dodds, D.A. Gudder, J. Phycol. 28 (1992) 415.
[15] F. Montechiaro, C.J. Hirschmugl, J.A. Raven, M. Giordano, Plant Cell. Environ. 29 (2006) 2198.
[16] D. Naumann, in: H. Gemlich, B. Yan (Eds.), Infrared and Raman Spectroscopy of Biological Materials, Marcel Dekker, New York, 2001, p. 323.
[17] P. Heraud, B.R. Wood, M.J. Tobin, J. Beardall, D. McNaughton, FEMS Microbiol. Lett. 249 (2005) 219.
[18] M.D. Abramoff, P.J. Magelhaes, S.J. Ram, Bophotonics Int. 11 (2004) 36.
[19] L.-P. Choo-Smith, K. Maquelin, T. van Vreeswijk, H.A. Bruining, G.J. Puppels, N.A.G. Thi, C. Kirschner, D. Naumann, D. Ami, A.M. Villa, F. Orsini, S.M. Doglia, H. Lamfarraj, G.D. Sockalingum, M. Manfait, P. Allouch, H.P. Endtz, Appl. Environ. Microbiol. 67 (2001) 1461.
[20] B.A. Whitton, Water Res. 4 (1970) 457.
[21] Y. Kimura, N. Mizusawa, A. Ishii, T. Yamanari, T. Ono, Biochemistry 42 (2003) 13170.
[22] B. Veuger, B.D. Eyre, D. Maher, Limnol. Oceanogr. 52 (2007) 1930.
[23] W.K. Dodds, Freshwater Ecology: Concepts and Environmental Applications, Academic Press, San Diego, CA, 2002, 569 pp..
[24] W.K. Dodds, B.J.F. Biggs, R.L. Lowe, J. Phycol. 35 (1999) 42.
[25] J.N. Murdock, W.K. Dodds, J. Phycol. 43 (2007) 449.
[26] W.K. Dodds, B.J.F. Biggs, J. N. Am. Benthol. Soc. 21 (2002) 2–15.